May 31st, 1:30 PM - 1:45 PM

An investigation of the velocity field over rippled sand bottom

B. Stachurska
Polish Academy of Sciences

R. Staroszczyk
Polish Academy of Sciences

DOI:10.15142/T3ZP4F

An investigation of the velocity field over rippled sand bottom

B. Stachurska[1], R. Staroszczyk[1]
[1] Institute of Hydro-Engineering, Polish Academy of Sciences,
Gdansk, Poland
E-mail: b.stachurska@ibwpan.gda.pl

ABSTRACT

Ripples at a sandy seabed are the consequence of the oscillatory movement of water particles. The ripples are the reason for the increase of the bed roughness of the bottom becoming an important factor in the sediment transport process. Better understanding of the processes taking place in the near-bottom flow field will allow an accurate description of the mechanism of the sediment transport. An experimental investigation of the velocity field over rippled sand bottom has been carried out in a wave flume of the Institute of Hydro-Engineering of the Polish Academy of Sciences in Gdansk. Measurements were performed using the technique of Particle Image Velocimetry. The velocity fields of the sandy sediment were measured in the region immediately over the flume bottom coated by sand ripples. The results obtained describe the instantaneous velocity fields of sediment particles along vertical and horizontal profiles at different spatial locations and at different phases of the oscillatory flow induced by free-surface water wave propagation. It has been demonstrated that the Particle Image Velocimetry technique of measuring the movement of sediment particles at the bottom proximity has proven as a reliable and sufficiently accurate method. The experimental data obtained will enable the validation of a numerical model which is currently developed.

Keywords: *Sediment movement, sand ripples, velocity field, PIV method*

1. INTRODUCTION

The study of the velocity field over rippled sand bed is fundamentally important for understanding sediment transport processes. The roughness of the bed increases as the ripples develop, which affects the near-bed water flows. Near-bed velocities of water particles depend on various factors, such a surface wave height, wave period or wave length. Consequently, the morphology of the seabed depends on the hydrodynamics of both water and sediment. The velocity fields can be calculated from theory or by numerical modelling, but obviously these methods should be based on the results from experiments and in situ observations.

In the literature on the subject there are descriptions of many experiments that have been carried out on water wave-generated sand ripples. One of the first was that conducted by Bagnold (1946), in which trays of sediment were oscillated in still water. Bagnold studied the variability of the geometry of sand ripples, and observed that the length of the ripples depends on the magnitude of the oscillation amplitude of water particles in close proximity to the bottom. The first important field research concerning ripples geometry was presented by Inman and Bowen (1962). Further extensive research on ripples geometry was conducted by Mogridge and Kamphuis (1972), Sleath (1975), Pruszak (1978) and Miller and Komar (1980). Boundary roughness of sandy beds was studied by Grant and Madsen (1982). These authors found that the bed roughness parameter is a function of the shear stress at the boundary. Sato, Mimura and Watanabe (1984) investigated experimentally the characteristics of the oscillatory boundary layer flow above rippled beds. These authors concluded that the velocity of the oscillatory boundary layer above the rippled bed is strongly influenced by vortices formed near the slopes of ripples. A very thorough experimental investigation of the mechanism of vortex generation and ejection from the ripple surfaces was carried out by van der Werf et al. (2007). They made detailed measurements of sediment particle velocities near bottom ripples in a series of experiments carried out in an oscillatory flow tunnel. Their results showed that the geometry of sand ripples gives rise to the formation of convective cells in the near-bed flows, resulting in a significant increase in the sediment particle velocities compared to those in free stream flows over flat beds. These authors also gave detailed insights into the mechanism of sand particle pick-up and the process of sediment transport in oscillatory flows.

The above experimental results by van der Werf et al. (2007) have been obtained by making use of a PIV (Particle Image Velocimetry) technique. This technique is based on the analysis of images of tracer particles seeded in water and observed within a thin sheet of fluid lit by laser light (Willert and Gharib 1991). The PIV

method, commonly used for over two decades for making measurements in one-phase fluid flows, can still be treated as a relatively new experimental tool for two-phase fluid flows, such as the flows of sediments suspended in water. This situation is due to some technical difficulties encountered in the implementation of the PIV technique in the case of two-phase flows, and due to problems with proper interpretation of measurement results. One of the first successful attempts to use the PIV method in experiments involving the motion of sandy sediments caused by water wave propagation belongs to Ahmed and Sato (2001). These authors investigated the dynamics of the bottom boundary layer and used the PIV technique to measure the volume flux of sand transported in sheet flow under asymmetric oscillations. Based on the measured velocity and sand concentration, the net volume flux was calculated. In another paper by Van der Werf et al. (2008) two different sediment models were tested and validated against the PIV velocity and sediment concentration measurements above full scale-ripples in regular oscillatory flow. Yang, Wang and Liu (2011) presented a method which enables simultaneous determination of the velocity fields of both phases in sediment transport problems by using the PIV with fluorescent tracer particles. Umeyama (2012), in turn, focused on surface waves propagating in water of finite depth and used the PIV technique to measure the water particle velocities and trajectories.

From among the above papers reporting the use of the PIV method for measuring sediment particle motion in water, only two (Ahmed and Sato 2001 and Umeyama 2012) were concerned with flows induced by free-surface gravitational waves propagating over a sandy bed. Hence, there is a need of further experimental investigation of the sediment transport phenomena in water due to surface wave propagation in order to enhance our understanding of fundamental mechanisms involved. The present work is an attempt in this direction. Another motivation of this work was to gather detailed experimental data sets that could be used to validate a numerical model (based on the Smoothed Particle Hydrodynamics method) which is currently developed by the authors.
The paper focuses on the measurements of instantaneous velocity fields of both sandy sediment particles near a rippled bed, and of water particles higher above the bed. In Section 2 experiments conducted in a wave flume with the use of the PIV technique are described. In Section 3 the results obtained and the data analysis are presented. Section 4 is devoted to the calculations of the thickness of the bottom boundary layer, based on the PIV data. Finally, in Section 5 some conclusions are presented.

2. EXPERIMENTAL SETUP AND DATA POST-PROCESSING

Experiments were carried out in a wave flume of the Institute of Hydro-Engineering of the Polish Academy of Sciences (IBW PAN) in Gdansk, Poland. The wave flume is 64 m long, 0.6 m wide and 1.4 m deep. Water waves were generated by a programmable piston-type wave maker. For the purpose of the experiments described here, part of the wave flume (of a length 6.07 m) was isolated from the rest of the flume. In this selected flume section, a container (cuvette) with sand was placed at 2 m downstream of the wave paddle (see Fig. 1).The sand was taken from a beach at a village of Sobieszewo (part of the Gdansk agglomeration). The median diameter of the sand grains was determined during a sieve analysis and was established to be equal to d_{50} = 0.257 mm.

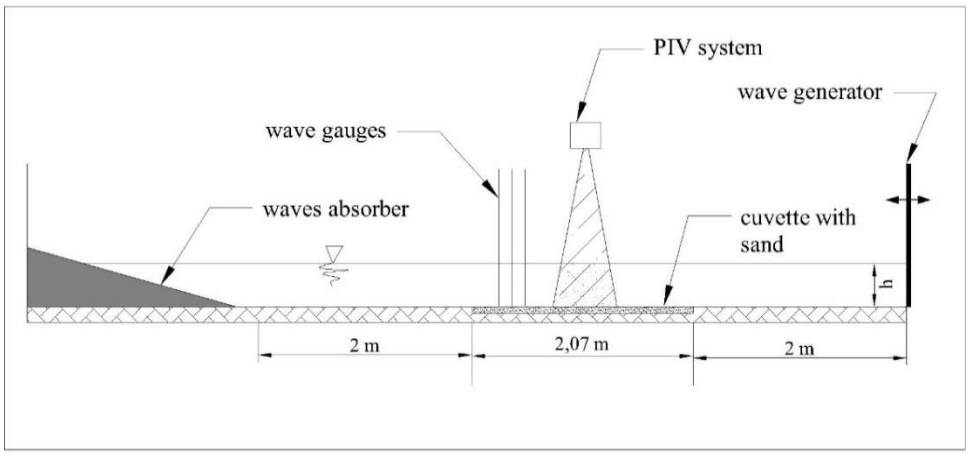

Fig. 1. Experimental setup.

The average water depth during the measurements was h = 0.3 m. Changes in the water free surface elevation were measured by a system of three wave gauges placed in the middle of the measurement area. The measurements were recorded with a sampling frequency of 100 Hz. In order to measure sand and water particle

velocities, a PIV system was applied. The PIV technique evaluates the instantaneous velocities through recording and analysing, at successive instances of time, positions of small tracer particles that are suspended in the fluid.

The main objective of the experiments was to determine the instantaneous velocity field in the near-bottom region. The main point of interest was to identify the velocity and direction of sand particles moving over rippled sandy bottom. During the PIV measurements, the laser light sheet was emitted from above the free surface of water in the flume. For recording successive images of sediment particle distributions, a high-definition digital video camera was used. The PIV system was supplied by *Dantec Dynamic*, and a *FlowSense EO 4M* camera was used during the measurements. In this system, the inter-frame time is 200 ns, and the sensor resolution is 2048 px × 2048 px. In our first experiments the water in the flume was seeded with glass hollow spheres. However, it turned out that the suspended sand grains in near-bed region acted as the seeding agent. The PIV post-processing was carried out by using the PIVlab1.4 software (Thielicke and Stamhuis 2014).

In the measurements, surface waves with a period of $T = 1.5$ s and a height of $H = 0.1$ m were used. Before starting the PIV measurements, water waves were generated for approximately 30 min, so as to achieve a state of equilibrium of bed forms. The resulting ripples had a height of approximately 1.7 cm and a length of approximately 7 cm.

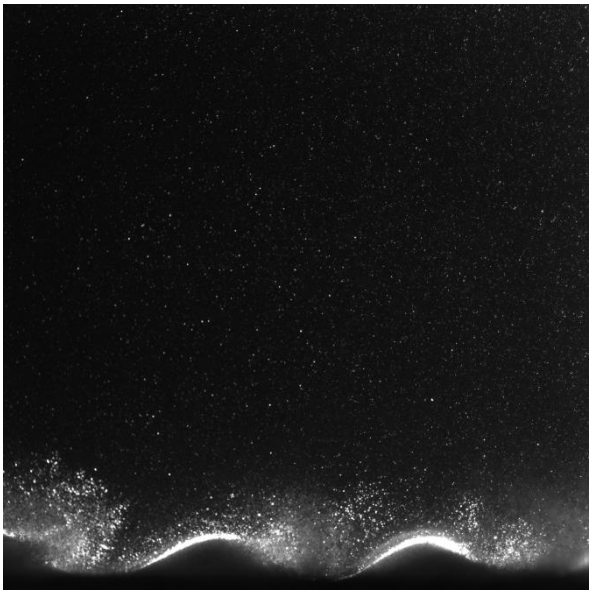

Fig. 2. Typical PIV image.

By analysing images (Fig. 2) recorded by the PIV camera, plots showing the instantaneous velocity field of sand particles were generated. The analysis of these data allowed the determination of the vertical and horizontal velocity profiles of the sand particles in the near-bed region.

3. VERTICAL AND HORIZONTAL VELOCITY PROFILES ABOVE THE RIPPLES

From the PIV experimental data, both the vertical and horizontal instantaneous velocity profiles were determined. Vertical velocity profiles were measured above the crest and trough of the representative bed form (Fig. 3a). A horizontal velocity profile was measured at a location just above the ripple crests (Fig. 3b), with the x-axis origin at the left border of the image and its direction to the right. The analysis of the vertical velocity distributions has been carried out for two cases: under the free-surface water wave crest, or under the water wave trough; that is, for two extreme cases of the water velocity magnitudes near the bed.

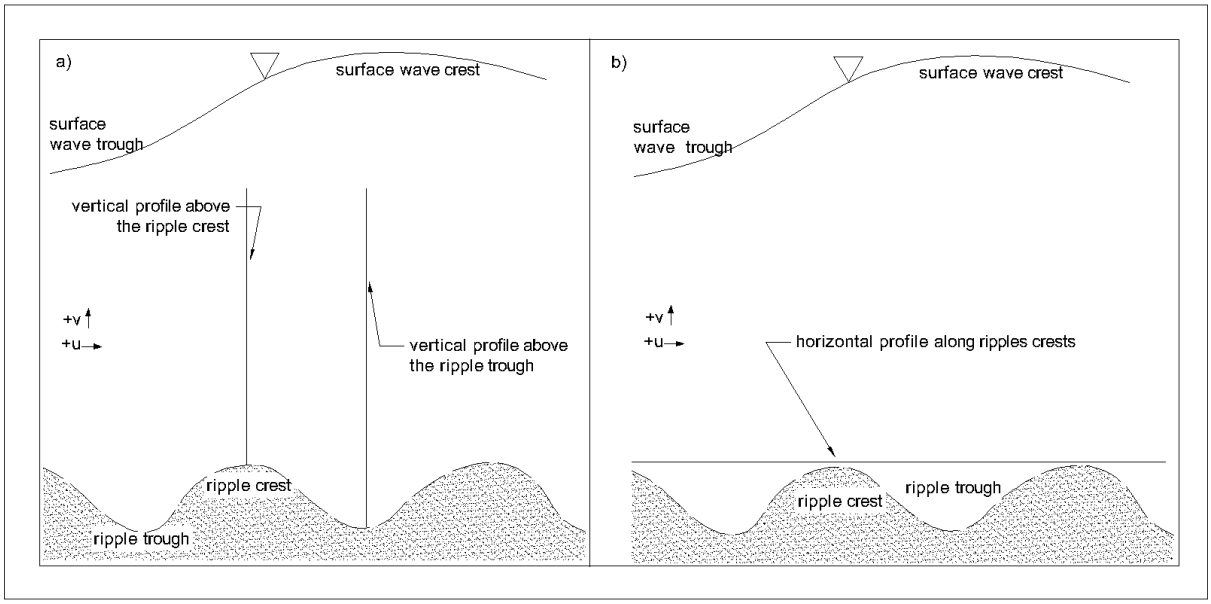

Fig. 3. Vertical (a) and horizontal (b) profiles above the rippled bed.

Figure 4 present the horizontal (u) component of the particle velocity. Fig 4a shows the vertical profile located in the ripple crest, and Fig 4b the vertical profile located in the ripple trough. The left plot in each figure shows the u-velocity profile measured with a surface wave crest directly overhead; the u-velocities profile on the right corresponds to surface wave trough directly overhead of the profile location.

Figure 4a shows that the near-bed extremum horizontal velocities are similar in magnitude in both situations and their maximum values vary within the range ±0.24÷0.23 m/s. Slightly higher are the velocities occurring during the transition of the wave trough. Above the region of the sediment moving layer, in a region of the free stream velocity, the horizontal velocity component is significantly smaller and has a value of approximately 0.16 m/s under the wave trough, and 0.12 m/s under the wave crest. Moreover, it was found that the sediment moving layer located in the near-bed region has a thickness 0.01 m at the time of the surface water wave trough transition, and 0.008 m at the time of the water wave crest transition.

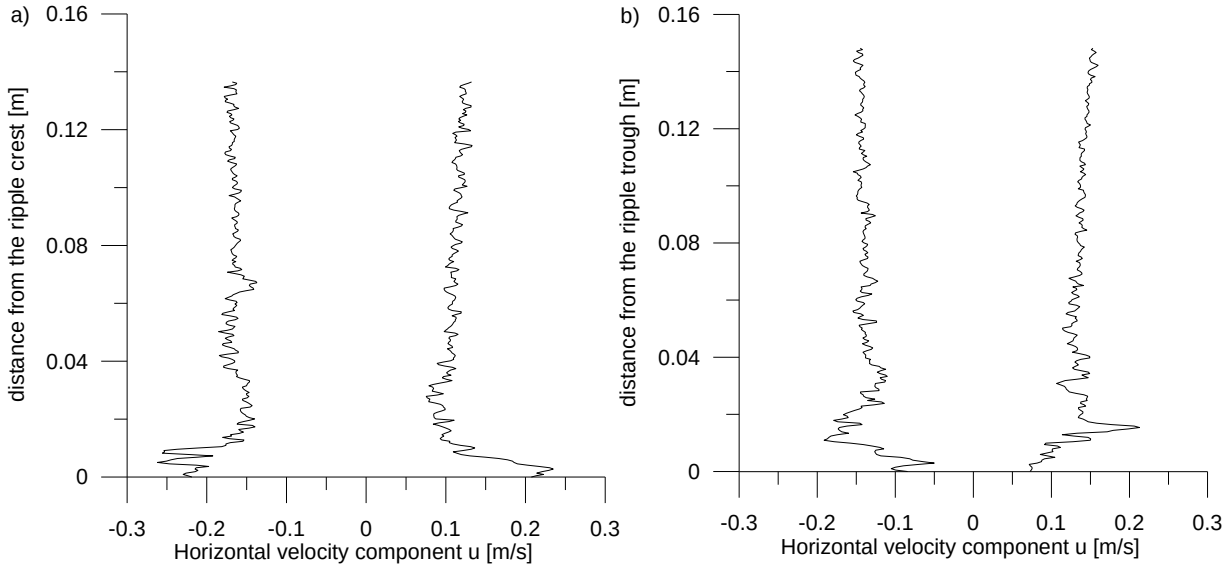

Fig. 4. Instantaneous horizontal velocity component distributions along the vertical profiles above the ripple crest (a) and above the ripple trough (b). For both locations shown are the velocity profiles under the surface water wave trough (left plot in each figure) and under the water wave crest (right plot).

Similarly, Figure 4b shows the vertical velocity profiles of the horizontal velocity component (u), but this time located at the ripple trough. Such a way of presenting the vertical profiles helps to determine the elevation above

the ripple trough at which the sediment movement under the action of surface wave begins. It was estimated that the thickness of this layer was 0.01m in case of the surface wave trough transition, and was 0.005 m in case of the wave crest transition. This finding is consistent with the results discussed above for the profile situated at the ripple crest (Fig. 4a). The wave-bottom boundary layer started at 0.01 m above the ripple trough surface at the time of the water wave crest transition, and at about 0.014 m at the time of the water wave trough transition. Moreover, it is seen that the near-bed extremum horizontal velocities, for the situation under the surface water wave trough, reach about 0.19 m/s (the left plot in Fig. 4b), and in the situation under the wave crest (the right plot in Fig. 4b) they are equal to about 0.2 m/s. It may seem a little surprising that the near-bed velocities are higher than those in the free flow field. This phenomenon, though, was already observed earlier by van der Werf et al. (2007), and results from the mechanism of the vortex generation and shedding off the sand ripple slopes, which considerably influences the flow within a region of about 1.5 ripple heights over the line of ripple crests.

The next step was to determine the vertical profiles of the vertical component (v) of the near-bed velocity. For this purpose, the same vertical profiles (Fig. 3a) as those described above were used. Figure 5 presents the vertical velocity distribution along a vertical profile located above the ripple crest. What is most characteristic for the two situations considered (the water wave crest and the wave trough transition) is the distinctive increase of the vertical velocity component in a near-bed region compared to the velocities occurring at higher locations in the free stream flow region. Under the water wave trough (Fig. 5a), the maximum vertical velocities in the near-bed layer of the moving sediment are 0.045 m/s, whereas under the wave crest (Fig. 5b) these velocities reach 0.05 m/s. The thickness of this wave-bottom layer was estimated as 0.008 m in the situation in the Fig. 5a, and 0.01 m in the situation in the Fig. 5b.

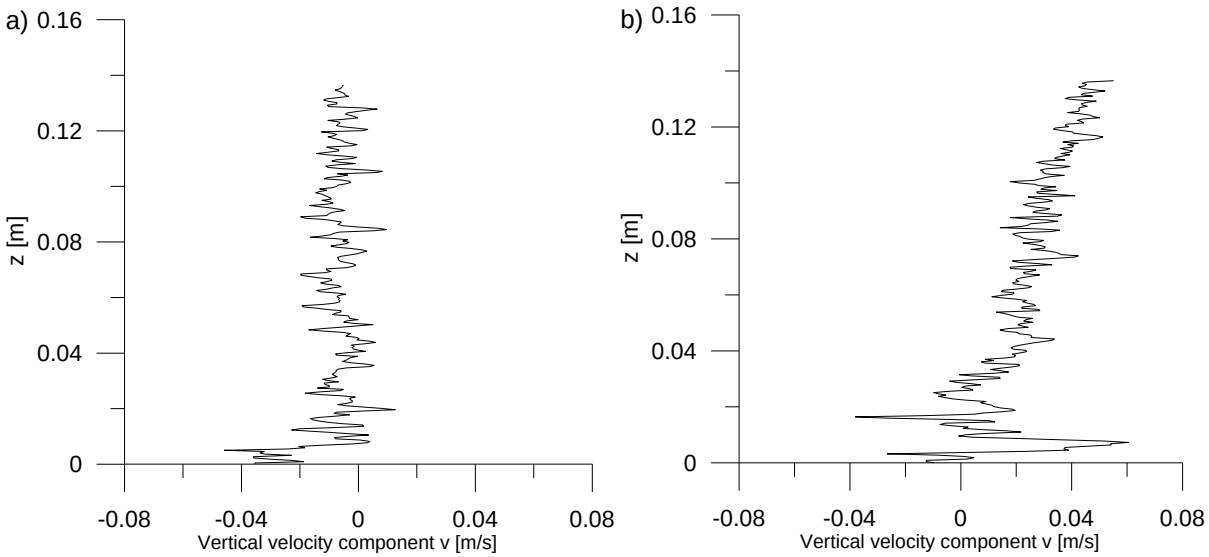

Fig. 5. Instantaneous vertical velocity component distributions along the vertical profile above the sand ripple crest: (a) under the water wave trough, (b) under the water wave crest.

From the vertical profiles located at the sand ripple trough (Fig. 6) some additional information about the vertical velocities of sand particles in the sediment moving layer was inferred. The thickness of the wave-bottom boundary layer under the surface wave trough (Fig. 6a) is about 0.03 m, and under the wave crest (Fig. 6b) it is about 0.02 m. The magnitudes of the vertical velocities in the moving sediment layer in both situations (under the surface wave trough and the wave crest) were similar and equal to about 0.05 m/s, which is compatible with the results plotted in Fig 5.

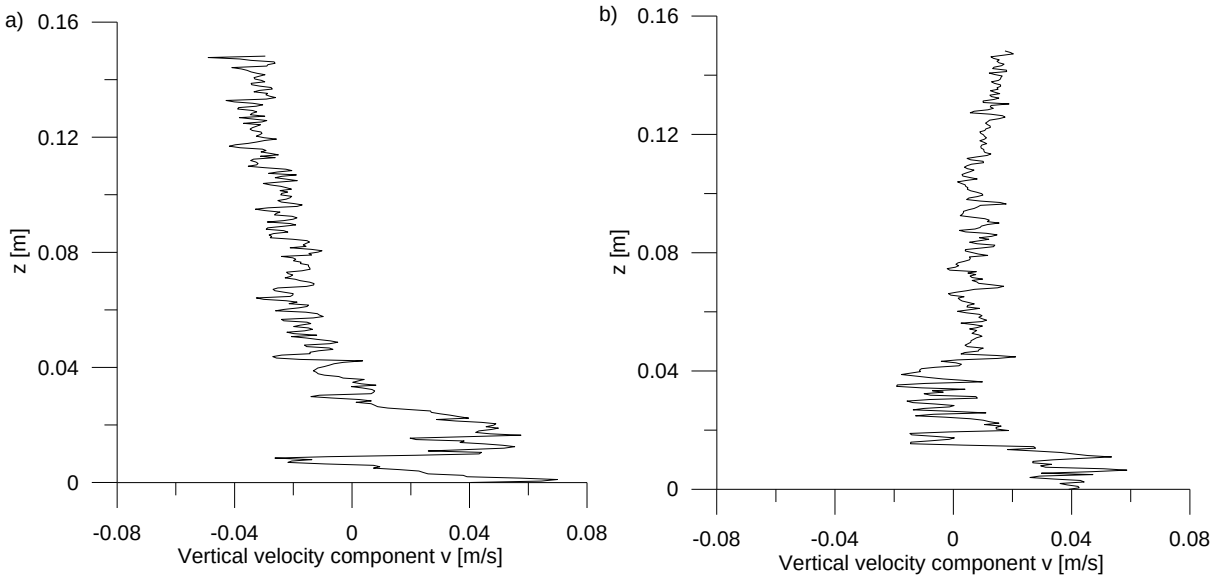

Fig. 6. Instantaneous vertical velocity component distributions along the vertical profile above the sand ripple trough: (a) under the water wave trough, (b) under the water wave crest.

Fig. 7 presents the vertical distributions of both sediment velocity components. Fig. 7a shows the distributions of the horizontal components (u), and Fig. 7b of the vertical components (v), at four different phases of a single free-surface water wave period T (t = 0 corresponds to the beginning of the flow period).

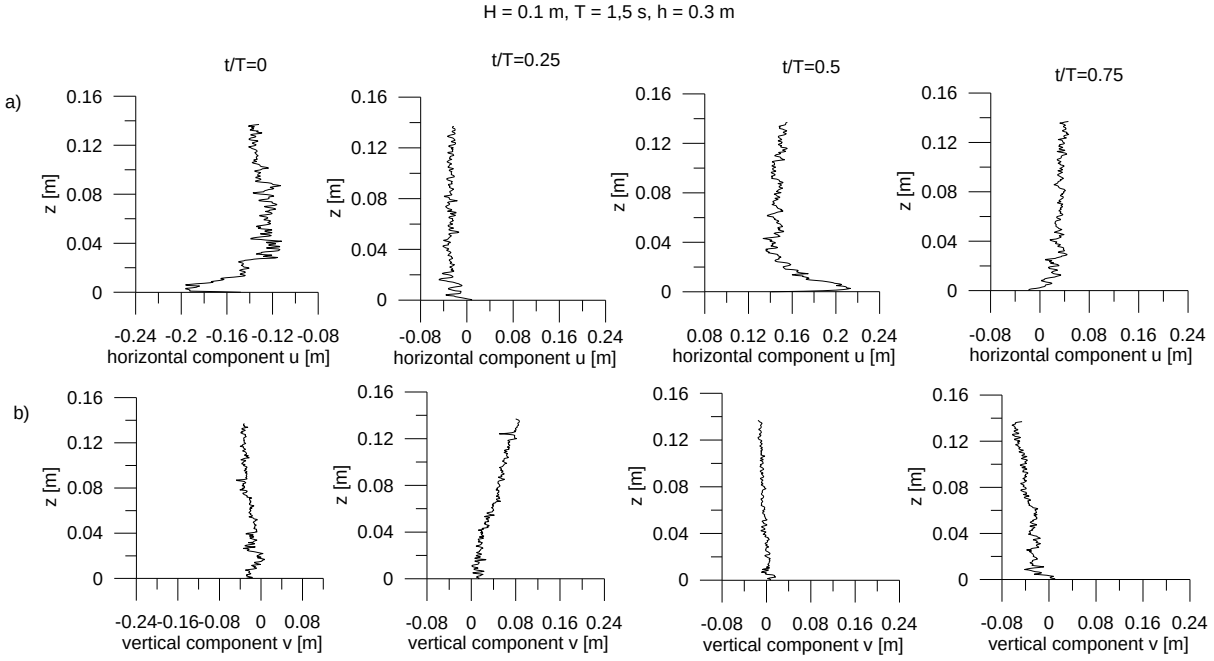

Fig. 7. Vertical profiles of instantaneous velocity distributions: (a) horizontal component (u), (b) vertical component (v), at four characteristic phases of a single free-surface water wave period.

The next stage of the PIV results analysis concerns the horizontal profile, which was located directly over the ripple crests (see Fig. 3b). The distribution of the horizontal velocity component (u) along that profile is presented in Fig. 8. It can be noted that the velocities u are clearly larger above the sand ripple crests than those over the ripple troughs. For instance, the mean values of u are 0.23 m/s over the ripple crests, compared to 0.08 m/s over the troughs. Moreover, both at the wave trough transition (Fig. 8a) and the crest transition (Fig. 8b), the values of the velocity components are comparable in magnitude along the horizontal profile.

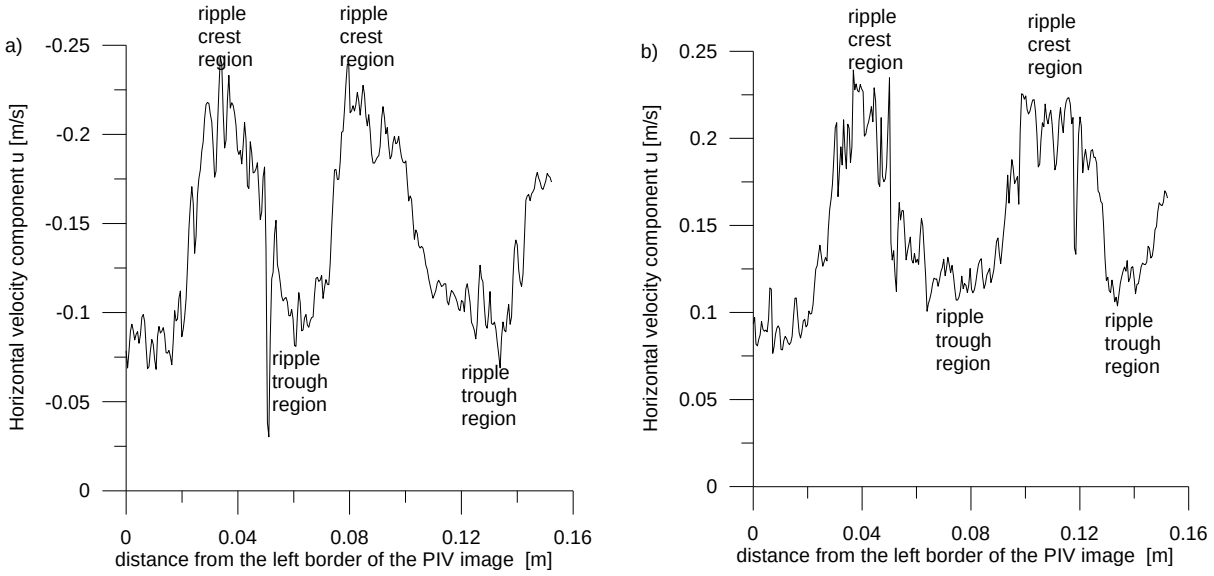

Fig. 8. Horizontal velocity component distributions along the horizontal profile: (a) under the water wave trough, (b) under the water wave crest.

Finally, the horizontal profiles of the vertical (*v*) velocity components are presented in Fig. 9. Also in this case, both during the free-surface water wave trough and the water wave crest transitions, the extremal measured values are quite similar in magnitude. Above the ripple troughs the vertical velocities are positive and vary from about 0.04 m/s to about 0.08 m/s. For comparison, over the ripple crests, the corresponding values are negative and change from –0.04 m/s to almost –0.08 m/s.

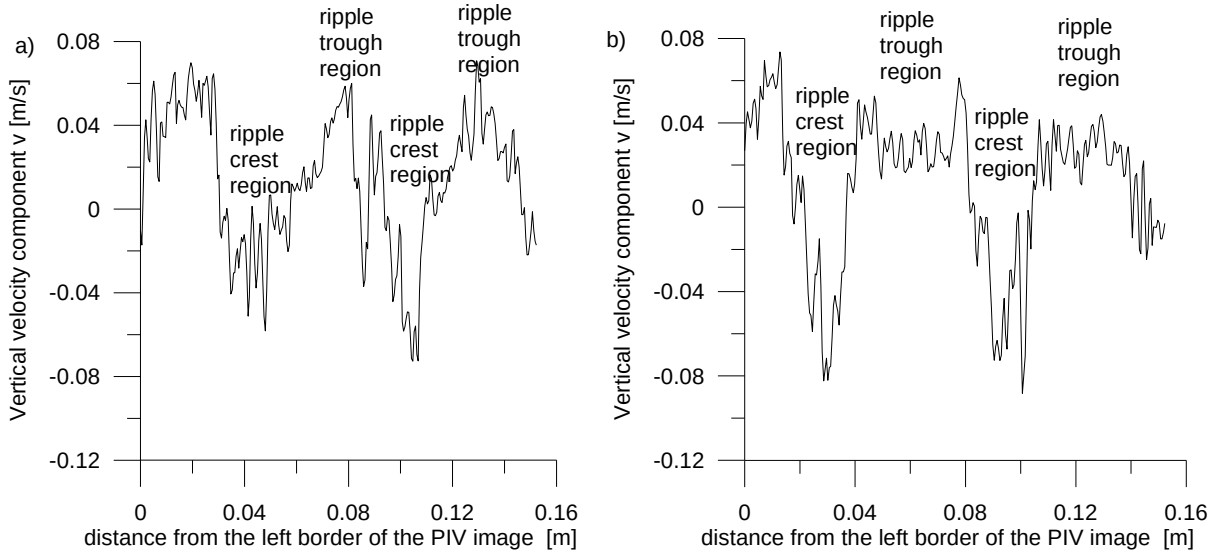

Fig. 9. Vertical velocity component distributions along the horizontal profile: (a) under the water wave trough, (b) under the water wave crest.

4. THICKNESS OF THE WAVE-BOTTOM BOUNDARY LAYER

The important part of the flow is the bottom boundary layer. The latter is meant as the layer inside which the flow is significantly influenced by the bed. The thinner the bottom boundary layer is, the larger shear stress is at a given flow velocity (Nielsen 1992). In this study, laboratory observations of the near-bed velocity are used to evaluate the thickness of the wave-bottom boundary layer (Fig. 10). As already noted, in a layer immediately above a rippled bed, the sand dynamics is dominated by the mechanism of vortex formation and shedding above the ripple slopes (van der Werf et al. 2007).

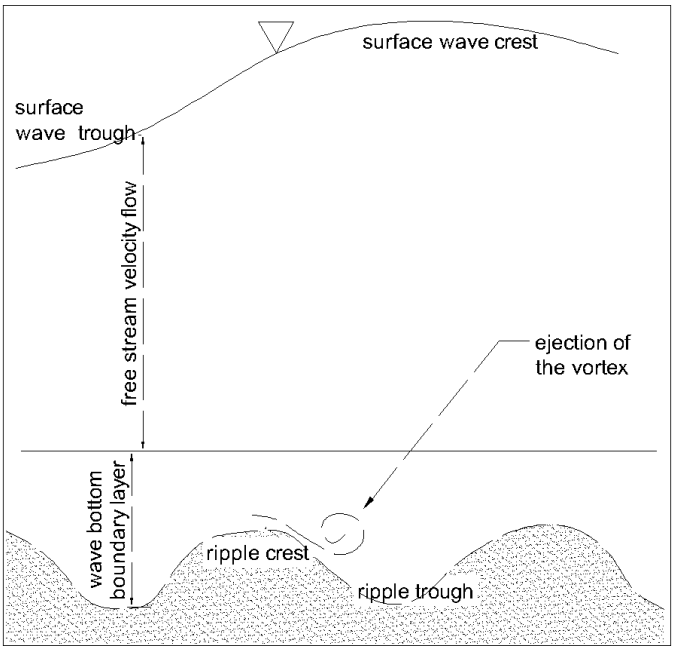

Fig. 10. Near-bed region with wave-bottom boundary layer.

In order to determine the thickness of the wave-bottom boundary layer, a formula proposed by Nielsen (1992) is used, which is exact for the case of simple time-harmonic flows:

$$\delta = \frac{1}{2}\frac{u}{\omega} f_w \tag{1}$$

where δ denotes the layer thickness, u is the horizontal velocity amplitude of the fluid occurring just above the boundary layer, ω is a wave angular frequency, and f_w is a so-called wave friction factor. The latter can be estimated by a method described in detail by Doering and Baryla (2002), based on formulae proposed by Nielsen (1992).

The first step to calculate the thickness of the wave-bottom boundary layer is to evaluate a grain roughness friction factor. This can be calculated by employing a formula by Swart (1974), which is expressed as:

$$f_{2.5} = \exp[5.213\left(\frac{2.5d_{50}}{u}\right)^{0.194} - 5.977] \tag{2}$$

where d_{50} is the median grain diameter of the sediment.

To measure the force exerted by fluid on a sediment particle during the surface wave transition, a dimensionless quantity is used, known as the mobility number, Ψ. The total disturbing force acting on a sand particle at the bed is approximately proportional to the square of the horizontal velocity amplitude u and the ratio between this disturbing force and the stabilising force due to gravity (Nielsen 1992). Hence, the number Ψ is defined by the equation:

$$\Psi = \frac{(u)^2}{(s-1)gd_{50}} \tag{3}$$

where s is the density of the sediment, and g is the acceleration due to gravity.

The sediment mobility number and the grain roughness friction factor define the grain roughness Shields parameter $\theta_{2.5}$ (Nielsen, 1992), expressed by the formula:

$$\theta_{2,5} = \frac{1}{2} f_{2.5} \Psi \tag{4}$$

The parameter $\theta_{2.5}$ is a dimensionless measure of the bottom shear stress, occurring in the flow over a sandy bed. When a bottom is covered by ripples, then $\theta_{2,5} < 0.25$, and it should be assumed that the hydraulic roughness of the bed is a function of the ripple height, its length and the grain roughness. To take into account the effect of the roughness due to the mechanisms of sand particles moving over ripples, a formula for the hydraulic roughness can be used:

$$r = \frac{8\eta^2}{\lambda} + 170 d_{50}\sqrt{\theta_{2.5} - 0.05} \tag{5}$$

in which η and λ are the ripple height and length, respectively.

The water under the surface wave interacts with the sandy bottom mainly due to shearing, which is measured by a shear stress τ. For this reason, the determination of the shear stress is an essential element in the calculation of the sediment transport. Generally, the friction factor of the wave is a function of the Reynolds number and the hydraulic roughness (r) of the bottom. Under certain conditions, the wave friction factor can be expressed in a simple way. For instance, if the bed is hydraulically smooth, than the friction factor f_w is a function of only the Reynolds number. If, in turn, the bottom is hydraulically rough, then f_w is a function of the bed roughness. It is assumed here that the bottom is hydraulically rough, which means that the boundary layer conditions are turbulent. In this case, the wave friction parameter is defined by:

$$f_w = \exp\left[5.5\left(\frac{r\omega}{u}\right)^{0.2} - 6.3\right] \tag{6}$$

where r denotes the hydraulic roughness of the bed, ω is the angular frequency. The wave friction factor, obtained from Eq. (6), can then be used to calculate the thickness of the boundary layer, as described by Eq. (1).

For the experiments described in this work, the ripple geometry was found to remain fairly constant, and could be described by the parameters η = 1.7 cm and λ = 7 cm. The median grain diameter d_{50}, as mentioned earlier, was 0.257 mm. For this case, the near-bed velocities in wave-bottom boundary layer were measured by the PIV technique, and the value adopted in the calculations was u = 0.24 m/s. With this information, the grain roughness Shields parameter ($\theta_{2.5}$), hydraulic roughness of the bed (r), and the friction factor (f_w) were found to be 0.16, 0.047, and 0.36, respectively. With these latter values, the thickness of the wave-bottom boundary layer, assuming rough turbulent conditions, was calculated to be equal to 1.04 cm. This result is consistent with that determined from the PIV measurements, wherein the thickness of the moving sediment layer in a wave-bottom boundary region, r, was approximately 1 cm, see the previous section.

5. CONCLUSIONS

The following conclusions can be drawn from the experimental observations presented in this paper:

(i) In the wave-bottom boundary layer, the maximum velocities near the ripple crest can be up to two times higher than the maximum free stream velocity. This is the result of the flow acceleration over the crest and the jet flow associated with the ejection of vortices on the slopes of the sand ripples (the mean velocity value in the near-bed region is 0.24 m/s, compared to 0.14 m/s in free stream flow).

(ii) The vertical velocities in the near-bed region vary from about 0.04 to about 0.06 m/s, and are strongly influenced by the presence of underlying sand ripples.

(iii) Bed forms significantly affect the near-bed sediment vertical velocities, leading to strong downward and upward local flows, depending on the local morphology of the ripples.

(iv) The thickness of the wave-bottom boundary layer (the sand active layer) was measured with a good accuracy, and its value was in accordance with the results of theoretical calculations.

6. ACKNOWLEDGEMENTS

Financial support for this research has been provided by the National Science Centre, Poland, under the contract no. UMO-2013/11/B/ST8/03818, and by the Institute of Hydro-Engineering of the Polish Academy of Sciences in Gdansk, Poland.

7. REFERENCES

Ahmed A.S.M. and Sato S. (2001). Investigation of bottom boundary layer dynamics of movable bed by using enhanced PIV technique. *Coastal Engineering*, 43 (4), 239-258.

Bagnold R. A., (1946). Motion of waves in shallow water, interaction between waves and sand bottom. *Proc. Royal Soc. London*, Series A, vol. 187, 1-15.

Doering J.C. and Baryla A.J. (2002). An investigation of the velocity field under regular and irregular waves over a sand beach, *Coastal Engineering*, 44, 275-300.

Grant W. D. and Madsen O. S. (1982). Movable bed roughness in unsteady oscillatory flow. *J. Geophys. Res*., 87, 469–481.

Inman D. and Bowen A.J. (1962). Flume experiments on sand transport by waves and currents, *Coastal Engineering Proceedings*, 8, 137-150.

Miller M.C. and Komar P.D. (1980). A field investigation of the relationship between oscillation ripples spacing and the near-bottom water orbital motions. *J. Sediment. Petrol*., 50, 183-191.

Mogridge G. R. and Kamphuis J. W. (1972). Experiments on ripple formation under wave action. *Proc. 13th Int. Conf. Coastal Engineering*, Vancouver, Canada, ASCE, 1123-1142.

Nielsen P. (1992). *Coastal Bottom Boundary Layers and Sediment Transport, Advanced Series on Ocean Engineering*, (4), World Scientific.

Pruszak Z. (1978). Procesy formowania się, rozwoju oraz zanikania małych form dennych w oscylacyjnym ruchu cieczy, *Rozprawy Hydrotechniczne*, 39, IBW PAN Publishing House (in Polish).

Sato S., Mimura N. and Watanabe A. (1984). Oscillatory boundary layer flow over rippled beds, *Proc. 19th Conf. on Coastal Engng.*, Houston, 2293-2309.

Sleath J.F. (1975). A contribution to the study of vortex ripples, *J. Hydraul. Res*., (13), 315-328.
Swart D.H. (1974). Offshore sediment transport and equilibrium beach profile, *Delft Hydr. Lab. Publ*., (131).

Thielicke W. and Stamhuis E.J., (2014). PIVlab – Towards User-friendly, Affordable and Accurate Digital Particle Image Velocimetry in MATLAB. *Journal of Open Research Software*.

Umeyama T. (2012). Eulerian–Lagrangian analysis for particle velocities and trajectories in a pure wave motion using particle image velocimetry. *Phil. Trans. R. Soc.* A 370, 1687–1702.

Van der Werf J.J., Doucette J.S., O'Donoghue T., and Ribberink J.S., (2007). Detailed measurements of velocities and suspended sand concentrations over full-scale ripples in regular oscillatory flow. *J. Geophys. Res.*, 112, F02012.

Van der Werf, Magar V. Malarkey J., Guizien K. and O'Donoghue (2008). 2DV modelling of sediment transport processes over full-scale ripples in regular asymmetric oscillatory flow. *Continental Shelf Research*, 28, 1040-1056.

Willert C. E. and Gharib M. (1991). Digital particle image velocimetry, *Original Experiments in Fluids*, 10, 181-193.

Yang B., Wang Y., Liu J. (2011). PIV measurements of two phase velocity fields in aeolian sediment transport using fluorescent tracer particles. *Measurement*, 44, 708-716.